Journal of Molecular Graphics and Modelling 52 (2014) 46–56

Contents lists available at ScienceDirect

Journal of Molecular Graphics and Modelling

journal homepage: www.elsevier.com/locate/JMGM

Structure-based drug design of small molecule SIRT1 modulators to treat cancer and metabolic disorders

Venkat Koushik Pulla[a], Mallika Alvala[a], Dinavahi Saketh Sriram[a,b], Srikant Viswanadha[b], Dharmarajan Sriram[a], Perumal Yogeeswari[a,*]

[a] Computer-Aided Drug Design Lab, Department of Pharmacy, Birla Institute of Technology & Science-Pilani, Hyderabad Campus, Hyderabad 500078, A.P., India
[b] Incozen Therapeutics Private Limited, Spectrum Discovery Zone, Alexandria Knowledge Park, Phase-I, Shameerpet, Hyderabad 500078, A.P., India

ARTICLE INFO

Article history:
Accepted 17 June 2014
Available online 24 June 2014

Keywords:
SIRT1 inhibitors
SIRT1 activators
High-through virtual screening
Docking
Cell-cycle analysis
Adipogenesis differentiation

ABSTRACT

Sirtuins comprise a family of deacetylase enzymes that catalyze the removal of an acetyl moiety from the ε-amino group of lysine residues within protein targets. Sirtuin 1(SIRT1), a NAD^+ dependent class III histone deacetylase is involved in a variety of human disorders such as obesity, type II diabetes, cancer and aging. Inhibition of SIRT1 could be useful for cancer treatment while activators can be useful for longevity and treating metabolic disorders. Hence we undertook an effort to design both inhibitors and activators using structure-based drug design techniques and report here the biological proof of concept. In this paper, we report diverse small molecule inhibitors with a potential to attenuate cancer growth designed based on high-throughput virtual screening and docking using the crystal structure of SIRT1. And small molecule activators with potential to suppress adipogenesis differentiation indicating their usefulness in obesity control was designed based on a homology model of SIRT1 activator domain.

1. Introduction

Sirtuins are evolutionarily conserved group of proteins that regulates varieties of functions such as metabolism, reproduction, development and cell survival. There are seven human sirtuins (SIRT1-7), which has different functions so as their sub cellular localization. Among all these sirtuins SIRT1 was well studied, with more than a dozen known substrates implicated roles in a wide range of cellular processes including cell survival and apoptotic pathways and hence this study was focused on designing activators and inhibitors against SIRT1 protein. Initially SIRT1 was known to be a nuclear protein and presumed it deacetylates only histone proteins, but later it was found that it shuttles between the nucleus and cytoplasm, displaying some important cytoplasmic functions as well. It was interesting to know that SIRT1 also deacetylate non histone targets, which include TAFI68 [TBP (TATA-box binding protein) associated factor I], p300, PACF [p300/cAMP-response-element-binding protein-associated factor], GCN5, MyoD, MEF2 (MADS box transcription factor enhancer factor 2), p19ARF, p53, HIC1, NF-κB, PGC1, PPAR, aP2, FOXO1,3a and 4, E2F1, p73, BCA3, Hes1 and Hey2, BCL11A, CTIP2, NCoR, SMRT, UCP2, and HIV-Tat [1,2].

1.1. Therapeutic importance of SIRT1 activators

Activators of SIRT1 can be useful to treat a variety of disorders like inflammation [3], neurodegeneration, regulation of glucose metabolism by regulating insulin secretion [4], regulating aging process and beneficial metabolic effects in calorie restriction [5]. It was interesting to know that SIRT1 is key mediator in caloric restriction pathway, which was a dietary regimen known to reduce diseases associated with age. This was further supported in knowing increased SIRT1 protein levels in various tissues of rodents following caloric restriction [5]. It was also found that activators targeted against SIRT1 have mimic the effects of caloric restriction, hence from past few years SIRT1 is been considered as a new weapon in the treatment of diabetes and obesity. SIRT1 activators were believed to ameliorate insulin resistance; interestingly resveratrol and SRT1720 (SIRT1 activators) has been shown to increase insulin sensitivity, mitochondrial content and glucose homeostasis in liver, skeletal muscle and fat tissues [5].

There were various SIRT1 activators reported previously, which include polyphenolic plant metabolites (STACs) of various structural classes like chalcones, flavones and stilbenes. Among all

* Corresponding author. Tel.: +91 40 66303515; fax: +91 40 66303998.
E-mail addresses: pyogee@hyderabad.bits-pilani.ac.in, pyogie_2000@rediffmail.com (P. Yogeeswari).

http://dx.doi.org/10.1016/j.jmgm.2014.06.005
1093-3263/

these natural products resveratrol was known to be most active in terms of its *in vitro* enzyme activity. In addition to the natural products there were several novel small molecule activators discovered, which include SRT2183, SRT1460 and SRT1720. These novel small molecules were structurally unrelated to the natural compounds previously reported. However there was wide room to discover structurally distinct SIRT1 activators, hence main objective of this study was to design novel SIRT1 activators through virtual screening of commercial available chemical databases.

1.2. Therapeutic importance of SIRT1 inhibitors

It was interesting to know that SIRT1 expression was known to be significantly increased in many cancers, like prostate cancer, acute myeloid leukemia and colon cancer [5]. Further to that increased expression of SIRT1 was also frequently observed in non-melanoma skin cancers. Based on the increased levels of SIRT1 in cancers, it was presumed that SIRT1 serves as tumor promoter. The role of SIRT1 in tumor promotion was supported by the study that showed that SIRT1 physically interact with p53 and attenuated p53 mediated tumor suppressor functions *via* deacetylating C-terminal Lys382 residue [5].

In addition to that, cells derived from SIRT1 deficient mice and cells treated with siRNAs against SIRT1 showed high levels of hyperacetylated p53. Hence SIRT1 was believed to represent an important target for cancer treatment.

Several inhibitors of SIRT1 were previously reported based on random biological assays that include nicotinamide [6], EX-527 analogs [7], splitomicin analogs [8,9,6] sirtinol analogs [10], cambinol [11], 2-anilinobenzamides [12], aristoforin [13] and various other compounds [14]. These compounds showed significant implications in treating cancer; hence this study was intended to discover novel small molecule inhibitors with distinct structural class.

1.3. Structural details of catalytic domain used in designing inhibitors

Several x-ray crystal structures of sirtuin proteins from bacteria (CobB and Sir2Tm), yeast (Sir2 and Hst2), archaea (Sir2-Af1 and Sir2-Af2), and human (SIRT2, SIRT3, and SIRT5) in several different liganded forms reveal a structurally conserved catalytic core domain. It adopts an elongated shape containing a large structurally homologous Rossmann fold domain (characteristic of NAD/NADH-binding proteins), a more structurally diverse, smaller, zinc-binding domain and several loops connecting the two domains [15]. Earlier when the three dimensional structure of SIRT1 was unavailable, homology model was built and the structure–function relationship of ligand binding motifs were reported which later paved way to the design of SIRT1 inhibitors [16,17]. Recently a crystal structure of SIRT1 catalytic domain at 2.5 Å resolutions (pdb id: 4I5I) bound to NAD and an inhibitor EX527 analog was released in the RCSB protein databank [18]. As per the crystal structure and reported papers it was known that the catalytic site formed at the junction of Rossmann fold and zinc binding domain, has two interfaces. The interface toward the zinc binding domain has two long helices along with two short helices that form a boundary around the pocket with aromatic and aliphatic side chains, because of which catalytic pocket facing the zinc binding domain was hydrophobic in nature, whereas the interface toward the Rossmann fold has hydrophilic in nature (characterized by having many hydrogen donors and acceptors) [16]. The catalytic pocket between large and small subdomains was usually divided into three sites, which was based on the binding of ribose, nicotinamide and adenine portion of the NAD^+. Among all the sites the location of adenine and ribose units was common in all the previously published articles [19–21], except the nicotinamide moiety, which was variable. It was usually believed that NAD^+ changes its conformation from a non-productive conformation to productive conformation. As described in the crystal structure (4I5I) the productive conformation nicotinamide was placed into the catalytic site. It has been known that flexible loop (269–295 amino acid residues) line the binding pocket. Relative to the large Rossmann fold this flexible loop has been reported to be involved in rigid body rotation of the zinc binding domain [22].

1.4. Structural information of allosteric site used in designing activators

Unlike catalytic domain the allosteric site or AROS (Active Regulator of SIRT1) binding site was not well characterized. There was no crystal structure available till date. In the year 2007 Kim et al., illustrated AROS an endogenous protein, which could activate the SIRT1 by interacting at allosteric site. As there was significant biological importance of SIRT1, in the past many investigators created model for allosteric site of SIRT1 [17,23], which revealed good structural details. Truncated mutational studies reported that amino acids from 183 to 225 were important for allosteric regulation of SIRT1 activity [24]. In addition to this when SIRT1 mutant (defective in AROS binding) was used in SIRT1 activation studies, AROS was unable to inactivate p53, which inferred that AROS has specific site for binding on SIRT1 [17]. From the model generated by the Costantini et al., it was inferred that at the interface of AROS and SIRT1 there were four aromatic, 1 positively charged and 5 negatively charged residues exposed. Few research investigators claimed that STACs activate the SIRT1 by forming complex with flouorophore-labeled peptides [25]. However in contrast to the above findings two reports published recently had resolved the controversy. One of the reports illustrated that they used mammalian acetylome microarray system to know whether natural deacetylation sites can respond to STACs activation. Resveratrol increased the SIRT1 activation for very few of the 7000 peptides used, which inferred that SIRT1 gets activated preferably when the peptide substrates consisted of large hydrophobic residues at C-terminal of acetyl-lysine. Thus fluorophore used in assays would be mimicking the hydrophobic residue at C-terminal of acetyl-lysine peptide [26]. These findings were further supported by other two other research groups, illustrating that the SIRT1 activation occur through STACs *via* allosteric site binding [27,28].

These data have triggered our interest to develop SIRT1 activators and inhibitors based on our drug design strategies involving virtual high-throughput screening and molecular docking techniques. Recently in our attempt to understand the role of SIRT1 in diabetes, we published a review highlighting various pathways in which SIRT1 was found to be a key sensor for changes in metabolism [29]. These SIRT1 modulators would be very much useful in the development of drugs for a variety of metabolic disorders. Thus in the present study utilizing the tools of structure-based drug design, we attempted to design novel SIRT1 activators and inhibitors based on the previously reported homology model and the available crystal structure with an inhibitor, respectively. The proof of concept was performed using various biological assays that included enzyme inhibition, activation, anticancer and adipogenesis to derive diverse set of SIRT1 inhibitors and activators useful for the treatment of cancer and metabolic disorders, respectively.

2. Experimental methods

2.1. Computational details

All computations were carried out on an Intel Core 2 Duo E7400 2.80 GHz capacity processor with memory of 2GB RAM

running with the RHEL 5.2 operating system. Software package used was the Schrodinger drug discovery consisting of modules for protein and ligand preparation and Glide for high-throughput virtual screening and docking. The LigPrep 2.5 [30] application from Schrodinger software package was utilized to build and energetically minimize structures and to add hydrogens and generate stereoisomers at neutral pH 7 using ionizer subprogram. Canvas 1.4 [31] chemoinformatics package that cluster molecules based on tanimoto similarities between a set of linear fingerprint descriptors was used to determine the structural diversity among the compounds and to select representative molecules from each clusters. QikProp module of Schrodinger was utilized to predict the drug likeliness properties of the hits.

2.2. Design of SIRT1 inhibitors

The crystal structure of SIRT1 bound with inhibitor (pdb id: 4I5I) with affinity data and having resolution of 2.5 Å was retrieved from the RCSB Protein Data Bank (PDB) and prepared using protein preparation wizard which was a part of the Maestro software package (Maestro, v9.2, Schrodinger, LLC, New York, NY). Bond orders and formal charges were added for heterogroups, and hydrogens were added to all atoms in the system. Water molecules in all structures were removed and the resulting structure was energy minimized. The commercial chemical database Asinex with over 600,000 compounds was processed through redundancy checking and Lipinski filters to select compounds that have better drugability. Database molecules were prepared using LigPrep (LigPrep v2.2, Schrodinger LLC, New York, NY) with Epik (Epik v1.6, Schrodinger, LLC, New York, NY) to expand protonation and tautomeric states at 7.0 (2.0 pH units). Conformational sampling was performed on all database molecules using the ConfGen search algorithm [32]. ConfGen sample conformations based on a heuristic search algorithm and energetic evaluations to efficiently explore diversity around rotatable bonds, flexible ring systems, and nitrogen inversions. We employed ConfGen with the OPLS_2005 force field and a duplicate pose elimination criterion of 1.0 Å rmsd to remove redundant conformers. A distance-dependent dielectric solvation treatment was used to screen electrostatic interactions. The maximum relative energy difference of 10.0 kcal/mol was chosen to exclude high-energy structures. Database ligands were docked into the binding site of the crystal structure with Glide 5.0 (Glide v5.0 Schrodinger, LLC, New York, NY). Glide energy grids were generated for each of the prepared complexes. The binding site was defined by a rectangular box surrounding the ligand in the X-ray structure. Ligands were refined using the "Refine" option in Glide, and the Glide SP (standard precision) and XP (extra precision) descriptor were chosen (Glide v5.7, Schrodinger, LLC, New York, NY). Default settings were used for the refinement and scoring. Initially we utilized the high throughput virtual screening (HTVS), scoring function to estimate protein–ligand binding affinities. Glide HTVS was faster and more tolerant to suboptimal fits than Glide SP and XP, making it better for comparison in this work. The center of the Glide grid was defined by the position of the co-crystallized ligand, NAD^+ was also included in the grid as there could be a possibility of van der Waals interaction with the inhibitors within the pocket [18]. Default settings were used for both the grid generation and docking. Compounds with best docking and GLIDE scores were then subjected to GLIDE SP and further XP screening.

2.3. Design of SIRT1 activators

From the mutational studies conducted by Milne et al. [24] and others it is known that AROS is placed between the N-terminal and allosteric binding site of SIRT1. The domain ranging from 114 to 217 amino acids was ideally considered as AROS binding site, hence homology model which was previously generated by Autiero et al., was used for docking and tested for its ability to screen the appropriate SIRT1 activators [17]. The commercial database (Asinex) ligands were docked into the allosteric binding site with Glide 5.0 (Glide v5.0 Schrodinger, LLC, New York, NY). Glide energy grids were generated for each of the prepared complexes. The high throughput screening and docking protocol was followed as presented in the inhibitor design methods. Docking result of known activator (Resveratrol) was compared with the shortlisted molecules.

2.4. In vitro SIRT1 assay

The enzyme inhibition studies were performed as per the instructions given in the kit (SIRT1 Fluorimetric drug discovery kit, Cayman) [33]. As per the supplier protocol all the reactions were carried in a reaction buffer that consisted of 50 mM Tris/HCl, pH 8.0, 137 mM NaCl, 2.7 mM KCl, 1 mM $MgCl_2$, 1 mg/cl BSA in the presence of 2% DMSO. Initially compounds were diluted in the reaction buffer with varying concentrations and were followed by the addition of enzyme to the total volume of 25 μL. The reaction was then initiated by the addition of 25 μL of 2× substrate solution containing 25 μM substrate and 500 μM of NAD^+ (co substrate). The whole 50 μL reaction mixture was incubated for 45 min at 37 °C, and later 50 μL of developer containing 2 mM nicotinamide was added to terminate the reaction. Fluorescence reading was measured using Perkin-Elmer VICTOR 1420 Multilabel Plate Reader with excitation set at 355 nm and emission measured at 460 nm. Besides we have determined the auto fluorescence of the test compound alone and the background noise of the substrate. The noise was later normalized and the percentage inhibition was calculated. Eventually IC_{50} was calculated using GraphPad Prism software. Assay was based on unique SIRT1 substrate/developer combination. The substrate usually consisted of 4 amino acids from 379 to 382 (Arg-His-Lys-Lys (Ac)) of human p53, which was tagged with aminomethylcoumarin (AMC). The fluorescence signal was generated in proportional to the amount of deacetylation of lysine in the substrate.

2.5. Cell culture and MTT assay

Cell lines used in the present study were procured from the American Type Culture Collection (ATCC, USA). CaCo2 (colon), LnCap (Prostate), MDAMB-231 (Breast), U937 (Lymphoma) and HEK-293 (Embryonic kidney cells) were grown in Dulbecco's modified Eagles's medium (containing 10% FBS in a humidified atmosphere of 5% CO_2 at 37° C). Cells were trypsinized when confluent from T75 flasks and seeded in 96-well plates in 200 μL aliquots at plating densities of 5000 cells/well. MTT (3-(4,5-dimethylthiazol-2-yl)-2,5-diphenyltetrazolium bromide) assay was then performed to determine the cell viability [34]. The synthesized compounds were tested for cytotoxicity in three different cell lines. The microtiter plates were incubated at 37 °C, 5% CO_2, 95% air and 100% relative humidity for 24 h prior to addition of experimental drugs. Aliquots of different drug dilutions were added to the appropriate microtiter wells resulting in the required final drug concentrations. Plates were later incubated for another 48 h, later 10 μL of 10 mg/ml concentration of MTT was added and incubated for 3 h at 37° C. At the end of incubation period formazon crystals were formed, the plates were then centrifuged and the media from microtiter plates were removed. Later plates were air-dried. The bound crystals were subsequently dissolved by adding 100 μL DMSO. The absorbance was then read on ELISA plate reader at a wavelength of 560 nm. Relative to the control wells the percent growth was calculated for each well. Sensitivity of the cells to the drug treatments was expressed in terms of IC_{50}/CC_{50} (HEK-293) it is the concentration of a compound at which 50% growth reduction

in growth is seen when compared to the control. The percentage of cells killed was obtained from the formula:

$$\%\,\text{Percentage cells killed} = \frac{100 - \text{Mean OD sample}}{\text{Mean OD day 0}} \times 100$$

2.6. Adipogenesis assay

Adipogenesis assay was performed as per the method followed earlier [35]. 3T3-L1 (Mice embryonic fibroblasts) was obtained from ATCC and they were grown in DMEM containing 10% FBS. Once the cells were confluent they were treated with test compound (DMSO in control wells) then the differentiation media containing DMEM, 10% FBS, 167 nM insulin, 0.5 mM isobutylmethylxanthine (IBMX), and 1 μM Dexamethasone was added and incubated for couple of days. After two days, differentiated media was replaced by media containing DMEM, 10% FBS and 167 nM insulin. Then the cells were further incubated for couple of days. It was followed by culturing the adipocytes for another 4 days with DMEM containing 10% FBS till more than 90% of the control wells were accumulated with fat droplets. Finally on day 6 they were fixed with formalin for 1 hr and stained with oil O red stain and visualized. Later the cells were washed with PBS and oil droplets in the cells were dissolved using DMSO and absorbance reading was then noted at 510 nm and quantified. Briefly principle of this assay was to stain fat droplets with oil O red stain, differentiation media added in the media induced adipogenesis, which resulted in accumulation of fat droplets. Cell groups which were treated with test compounds (SIRT1 activators) were presumed to reduce the adipogenesis, and reduced accumulation of fat droplets.

2.7. Cell cycle analysis

Cell cycle analysis was done as per the instructions given in the kit (Guava Cell Cycle Assay kit) [36]. After incubation with the test compound, cells were harvested and freezed in −20 °C with ethanol for overnight. Then DNA was stained with propidium iodide. Then the cell cycle cell cycle gates were set to a position in dot plot which corresponds to four markers, marker 1: G1 phase, marker 2: S phase, marker 3: G2/M phase and marker 4: sub-G0/G1. Principle of this assay was to stain the DNA using propidium iodide. At each phase of the cell cycle the DNA concentration was monitored using flow cytometer and thus percentage of cells at each phase can be determined. By performing this assay we could understand whether the cells were in normal growth phase or in apoptotic stage, usually it was known that cells undergoing apoptosis enter G0 phase. Hence if cells increased in G0 phase, it was inferred that test compounds induced apoptosis.

3. Results and discussion

3.1. Drug design of inhibitors and activators

As described in the material and methods crystal structure (4I5I) and homology model of AROS binding site developed previously [17] were used to screen the inhibitors and activators from the Asinex database (commercially available), respectively. To understand docking pose of inhibitor, the known inhibitor in crystal structure was redocked flexibly and rmsd (root mean square deviation) was compared with the pose of inhibitor in the crystal structure. The rmsd was 0.8479 Å, which inferred that the docking pose and grid conditions were well within the range (<2 Å) and could be considered to virtually screen any commercial database. In the case of homology model we have used the model generated by Autiero et al., for docking studies, they have done informative molecular dynamics studies and gave hints about allosteric site pocket [17], hence binding pocket as previously proposed was considered and grid was generated covering the following amino acids ASP166; ARG167; SER169; HIS170; ALA171; SER172; SER173; SER174; ASP175; TRP176; PRO184; TYR185; PHE187; VAL188; HIS191; LEU192. The importance of this region was further supported by truncation mutations studies conducted by Milne et al., which defined the amino acids from 180 to 220 to be important in modulating the SIRT1 through allosteric interaction [24].

The general protocol followed for both inhibitor and activator design were that an initially HTVS (high throughput virtual screening) docking and then secondary SP docking was done, by which the survivors from these docking studies were further run through XP docking along with known reported ligands. Based on the docking score, hydrogen bond, π–π stacking interactions, top five ligands of both inhibitors (**I1–I5**) and activators (**A1–A5**) were shortlisted and their structures are presented in Fig. 1.

3.2. Profile of the designed inhibitors

The finest of these screened ligands along with hydrogen bond interactions of inhibitors are depicted in Table 1. Known inhibitors were utilized to validate and compare the results for better selection. The hits were found to show similar interactions as that of crystal ligand (**CL**) or were found to show similarity with regard to known inhibitors like salerimide, splitomycin, EX-527 and sirtinol (Table 1). All the top shortlisted inhibitors showed π bonding with Phe-297 or Phe-273, which strongly support the statement of Zhao et al. that inhibitors interact with SIRT1 primarily through hydrophobic interaction and fixed deep in the active site behind the nicotinamide and second ribose of NAD^+ [18]. Considering the docking position of most potent compound (**CL**) [18], it can be inferred that it interacted well with the available H-bond acceptor

Table 1
Glide docking score, important amino acids and gold fitness of shortlisted inhibitors.

Inhibitors	Glide score	H bond	Amino acid involved in interactions with ligand	Gold score
I1	−7.568	2	Gln-345, Val-412, Gln-320, Phe-297 (π bonding)	62.34
I2	−6.413	2	Asn-346, Asp-348, Pro-271, Phe-293 (π), Phe-297 (π)	43.95
I3	−5.043	1	Gln-345, Phe-297 (π), Phe-273 (π)	47.17
I4	−3.298	0	Phe-297 (π)	53.88
I5	−4.617	0	Gln-345, Phe-273 (π)	48.34
Saleremide	−4.514	0	Phe-297 (π)	47.99
Splitomycin	−8.262	0	Phe-297 (π)	33.57
Sirtinol	−3.786	0	Phe-273 (π)	50.69
CL[a]	−8.979	3	Asp-348, Ile-347, Gln-345, Phe-273 (π), Phe-297 (π)	45.47
EX-527[b]	−9.132	4	Asp-348 (2), Ile-347, Gln-345	29.78

[a] CL represents crystal ligand from pdb id: 4I5I.
[b] EX-527 is from Ref. [7].

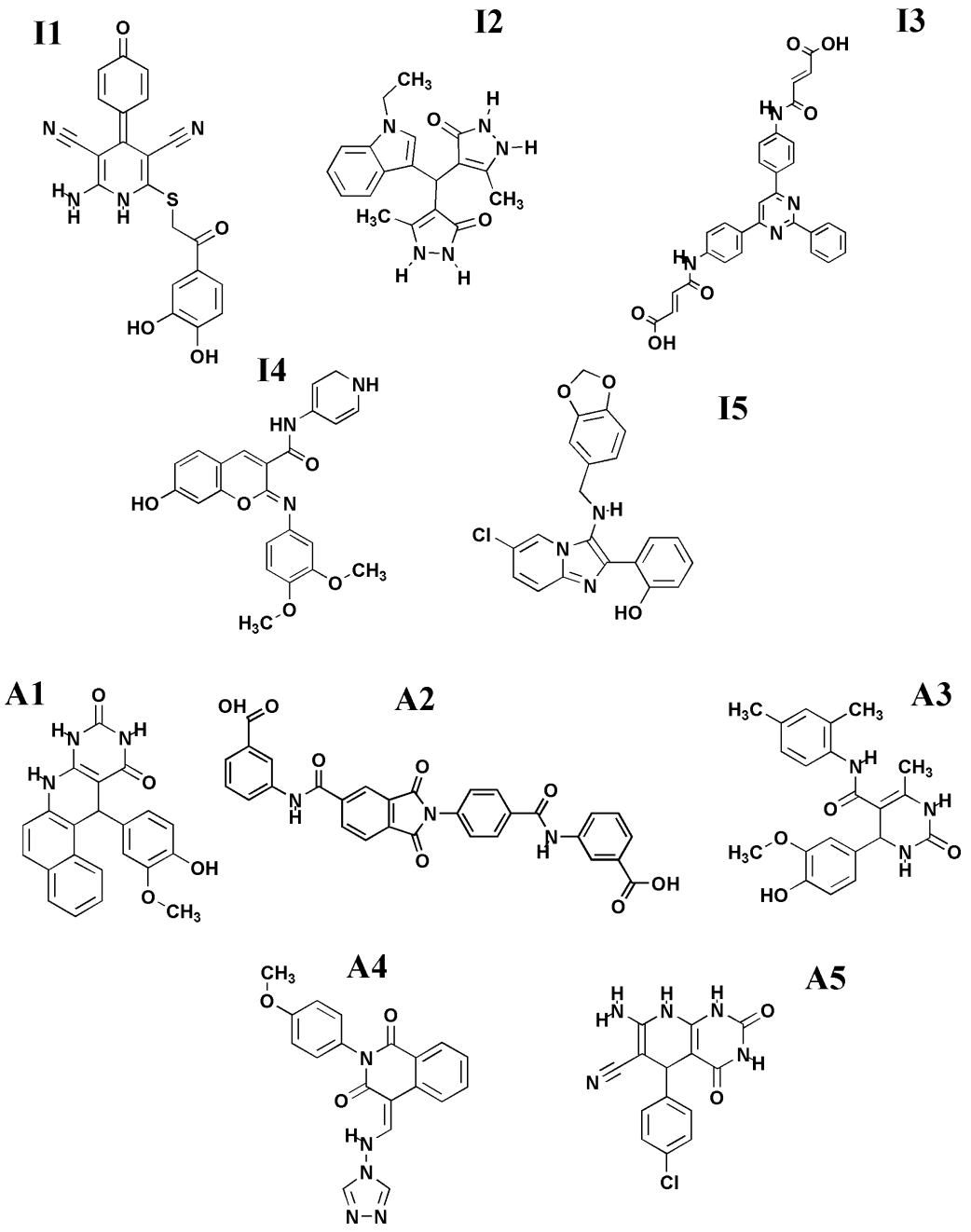

Fig. 1. Structures of shortlisted inhibitors (**I1**–**I5**) and activators (**A1**–**A5**) from Asinex database.

and donor sites. The hydrophobic site of catalytic pocket was found to interact with the aliphatic and aromatic parts of the inhibitor as presented in Fig. 2. From the docking pose it was known that catalytic pocket with inhibitor has extensive H-bonding. As the amide (—NH_2) moiety of inhibitor facing the carboxyl group of Asp-348 donate hydrogen in addition to that the carbonyl oxygen of inhibitor showed hydrogen bonds with the NH of Asp-348 and Ile-347. Further to this, NH group of indole ring act as H-bond donor to the carbonyl oxygen of Gln-345. Down to this H-bond network, a flexible loop lines the catalytic pocket in a conformation which was triggered by the NAD^+ binding [22,37]. From the figure it can be seen that Phe-273 oriented into the pocket and prevent or restrict the binding of large size ligands. Toward the other side chorine group of aromatic ring of inhibitor lie adjacent to the Phe-297. This binding conformation was exactly similar to the model proposed by Huhtiniemi et al. [16].

We compared the docking pose of the known inhibitor (**CL**) with the finest hits filtered through docking studies. It was observed that hydrophilic moieties were adjacent to the hydrogen bond donor and acceptor residues (Fig. 2). In case of **I1** the two-hydroxyl groups were precisely fixed and oriented adjacent to the Gln-345 and Val-412, whereas the hydrophobic head group of phenyl ring was facing toward the Phe-297. The other two rings of this compound were not allowing these rigid planar rings to move or rotate flexibly. This prevented the proper fixing of the hydrophilic moieties (oxo, cyano and amine groups) adjacent to the Asn-346 and Ile-347. In the case of **I2** we could see two identical 2,3 diazole rings which showed both hydrogen acceptors and hydrogen donor moieties. Hence these moieties on one of the diazole rings were freely bound with Asn-346 and Asp-348, while benzopyrrole, the hydrophobic moiety was oriented away from the hydrophilic pocket. With regard to **I5**, chlorine at pyridine ring was oriented similar to chlorine on the known

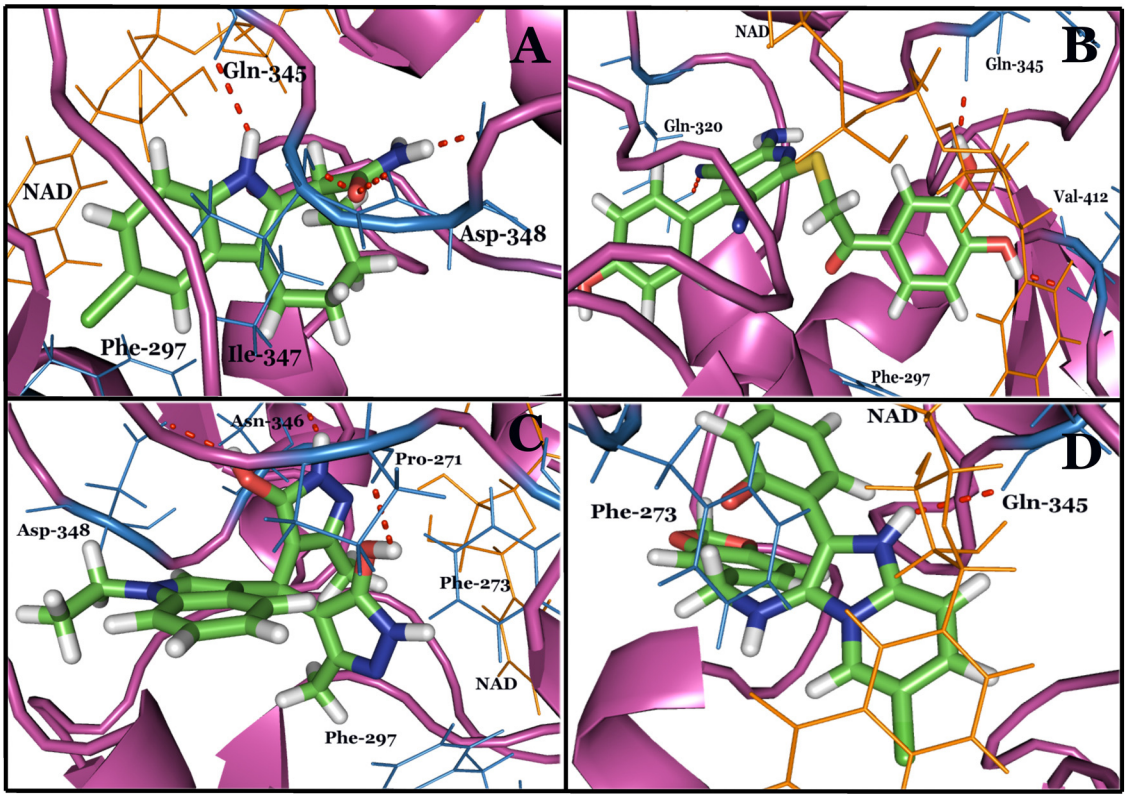

Fig. 2. Depicting the binding pose of inhibitors in the active site pocket. A B C and D represent **CL**, **I1**, **I2** and **I5**, respectively. The red color bonds indicate the hydrogen bonds between ligand (in sticks) and amino acids (in blue lines). The NAD in the active site pocket was represented in orange color.

inhibitor (**CL**) adjacent to the Phe-297. Further the hydroxyl group was found in ortho position, which was away from the Gln-345 and Asn-346. If it would have been in the para position there could have been a chance for the inhibitor to make bonding firmly with Gln-345 and Asn-346 residues. Hence we observed only π bonding with Phe-273. The inhibitors showed π bonding with Phe-297 or Phe-273, thus resulting in extended conformation of NAD^+ binding lengthwise across the mouth of the binding site, which sterically obstructs the productive binding of substrate.

3.3. Profile of designed activators

On the other side docking of known activator (Resveratrol) was compared with the shortlisted molecules (Table 2). The compounds were shortlisted based on docking score, hydrogen bonds and important amino acid residues contributing to the allosteric site of the protein. The docking pose of these molecules showed similar interaction pattern as proposed in previous literature [17,23]. The interactive residues observed in allosteric binding region mainly showed aromatic and charged residues, which inferred that these activators were stabilized by the electrostatic and stacking interactions. The interactions of resveratrol illustrated that the hydroxyl groups were important for interactions with Asp-216, Arg-167 and Asp-166. Besides, the complex formed between the resveratrol and SIRT1 was not as stable as the shortlisted molecules (**A2**, **A3** and **A4**). This could be attributed to the presence of extra hydrogen bonds (3 in case of resveratrol, 5, 6 and 5 with **A2**, **A3** and **A4,** respectively). Especially the compound **A2** was straight as resveratrol and showed advantage in interacting with Ser-174, Asp-175, Arg-167 and Glu-190 that gathered a good docking score. The other major advantage of this molecule (**A2**) was size, as it was sufficiently big enough to occupy the entire groove of the active site pocket as presented in Fig. 3. The conformation of other two shortlisted molecules (**A3** and **A4**) were bit different (branched conformation) but the pharmacophore moieties were well suited to the pocket having charged residues, hence they could show more hydrogen bonds when compared to resveratrol.

All the finest hits (both inhibitors and activators) were procured from Asinex database, and *in vitro* enzymatic assay was performed using cayman kit using recombinant human SIRT1 and further tested *in vitro* in disease models.

3.4. In vitro enzyme assay

During the *in vitro* enzymatic assay we employed different controls like with and without substrate to reduce the background signals. We first screened for the enzyme activity assay to prove the concept of drug design. While screening we utilized Resveratrol (100 μM) and suramin (3 μM) as reference compounds for activator and inhibitor comparison, respectively. The concentrations were fixed as the EC 1.5 and IC_{50} values were near about 100 μM and 3 μM, respectively. As resveratrol was a known activator hence the increase in the fluorescence was compared with the other test compounds and in contrast suramin which was an inhibitor could act as a negative control which decreases the fluorescence (Fig. 4). Five compounds from the inhibitor class were found to be promising and there hill plots were depicted in Fig. 5. For comparison we had included the IC_{50} data of known inhibitors like suramin, sirtinol, **CL**, and EX-527 as reported in the literature. From the results it was inferred that compound **I1** was considered as most potent inhibitor with IC_{50} of 16.35 ± 0.975 (Table 3). In the case of activators it was **A2** which showed increase in the fluorescence at all the three concentrations compared to the other test compounds. From the results it was also clear that these compounds have shown moderate activity at 10 μM. Hence the EC1.5 values would be >10 μM though not calculated.

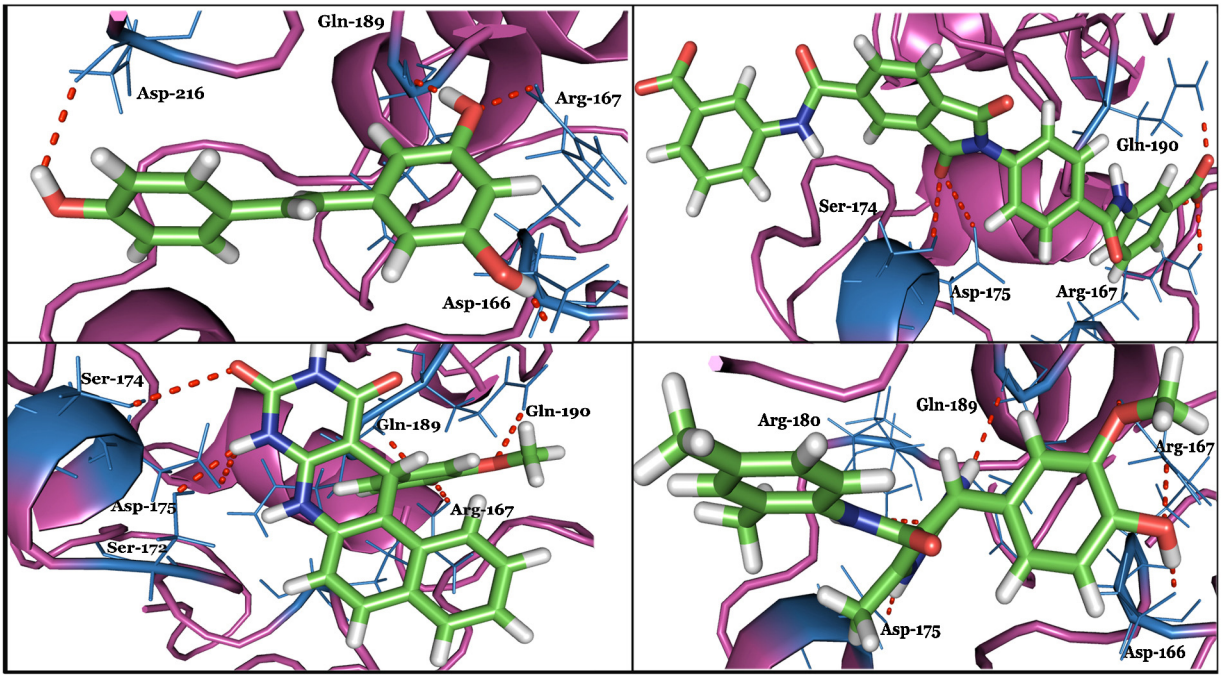

Fig. 3. Depicting the binding pose of activators in the AROS binding pocket. A B C and D represent **resveratrol**, **A2**, **A3** and **A4**, respectively. The red color bonds indicate the hydrogen bonds between ligand (in sticks) and amino acids (in blue lines). (For interpretation of the references to color in text, the reader is referred to the web version of this article.)

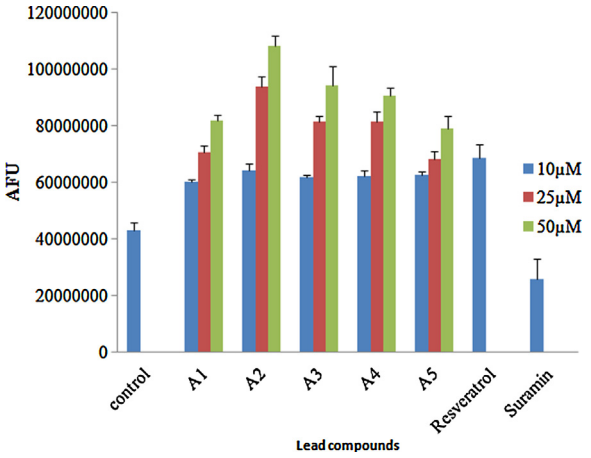

Fig. 4. Fluorescence values of activators at three different concentrations, where the controls represent the reaction without any test compound. Resveratrol was tested at 100 μM and suramin tested at 3 μM.

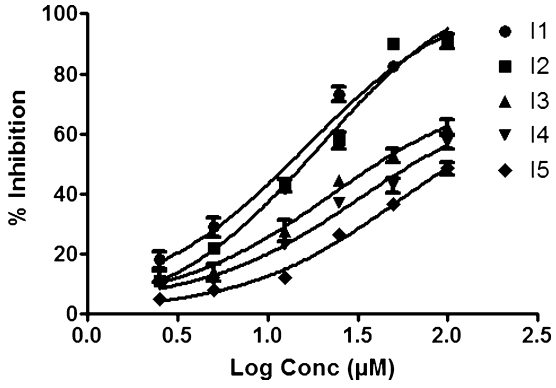

Fig. 5. Illustrating the percentage inhibition at different concentration of test compounds.

3.5. *In vitro anticancer assay*

As we know that SIRT1 has been reported to be over expressed in many cancers, it was proven before that SIRT1 inhibitors could specifically be used in cancer treatment; hence the anticancer activity was studied using MTT on four cell lines. All the top 5 inhibitors with IC_{50} values were considered for this study and the results are presented in Table 4. For comparison we utilized standard drug as gemcitabine in various concentration and the GI_{50} is reported in Table 4. From the results it was inferred that most of the compounds were showing GI_{50} of less than 5 μM in almost two of the cell lines and all the compounds showed GI_{50} of less than 1 μM in prostate cancer cell line. From this we could intrigue

Table 2
Glide docking score, important amino acids and gold fitness of shortlisted activators.

Activators	Glide score	H bond	Amino acid involved in interactions with ligand	Gold score
A1	−4.97	6	Ser-172, Arg-167, Gln-189, Gln-190, Asp-175, Ser-174	46.04
A2	−5.48	5	Ser-174, Arg-181, Gln-190, Arg-167, Asp-175	65.53
A3	−4.67	5	Asp-175, Asp-166, Arg-167, Arg-180, Gln-189	49.63
A4	−2.464	1	Arg-167	45.43
A5	−2.19	2	Gln-189, Arg-167	45
Resveratrol	−3.917	3	Gln-189, Arg-167, Asp-166	43.2

Table 3
Depicting the IC_{50} values of *in vitro* hSIRT1 inhibition.

Compounds	IC_{50} (μM)
I1	16.35 ± 0.975
I2	19.59 ± 2.347
I3	22.15 ± 3.563
I4	52.92 ± 4.270
I5	32.03 ± 11.907
CL	0.067[a]
EX-527	2.7[a]
Sirtinol	130[b]
Suramin	2.5[c]

[a] The IC_{50} values of CL and EX-527 were from Ref [7].
[b] The IC_{50} value of Sirtinol was from Ref [10].
[c] The IC_{50} value of Suramin was from Ref. [10].

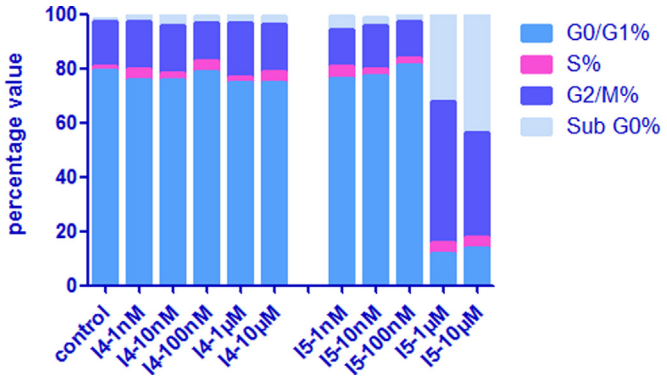

Fig. 6. Showing the percentage of different cell phases after treating LnCap with two test compounds (I4 and I5) at five different concentrations.

that these molecules best acts on prostate cancer. We further performed cell cycle analysis at five different concentrations for two compounds (**I4** and **I5**). We selected these compounds as they showed GI_{50} less than 100 nM in prostate cancer. There were three compounds that showed GI_{50} value less than 100 nM (**I3**, **I4** and **I5**). Among the three, **I3** showed less potency against MDAMB cell line with GI_{50} value of 50 μM, whereas the other two showed 1.2 μM and 15.1 μM, respectively. The other reason for comparing the GI_{50} values of LnCap and MDAMB were based on the literature evidence of SIRT1 specifically overexpressed in these two cell lines and they were well characterized. From the cell cycle analysis data (Fig. 6) we could understand the percentage of cells in each phase and from the results it can be inferred that cells treated with compound **I4** showed similar percentage of cells when compared to the control (untreated) at different cell phases, whereas compound **I5** showed significant difference at 1 μM and 10 μM concentrations. It was also clear that cells entering into sub G0 phase were found to have increased from 1 μM to 10 μM, which clearly indicated that cell undergoing apoptosis had increased. Thus from this study **I5** was considered as the most potent anticancer drug among the five. To understand the cytotoxic characteristics of compound **I5**, we tested on HEK-293T cell line (Human embryonic kidney cell line) at different concentrations. The CC_{50} (cytotoxic concentration 50) was found to be 40.12 μM, which was comparatively higher (10–100 times) than the GIC50 against 5 cancerous cell lines. Hence it could be inferred that compound I5 was not toxic on non-cancerous cell lines and was found to be more specific to cancerous cell lines.

If we compare the results from docking, *in vitro* enzymatic assay and cell based assays we could understand that the compound **I5** had shown moderate activity in both docking studies (docking score −4.617) and *in vitro* enzyme based studies (IC_{50} – 32 μM) compared to the compound **I1**, though it was found to show good interactions (docking score −7.568) and better IC_{50} (16.35 μM) among the rest. This could be due to the fact that compound **I5** could be acting through other mediators including SIRT1. As we knew that sirtuins were evolutionarily conserved and there were various sirtuins in humans (SIRT1-7) which were closely linked. They differed in amino terminal and carboxy terminal protein sequence flanking the catalytic core, which meant that the catalytic core, was more conserved. In the present study we targeted the catalytic core of SIRT1, which may be similar with corresponding catalytic core of other sirtuins. Hence the compound **I5** could be acting through other sirtuins resulting in low GIC_{50} compared to others.

As stated in the introduction we know that SIRT1 has many targets, which include various transcription factors like p53, E2F1 and various other transcription factors belonging to FOXO family. This could be inferred that inhibiting SIRT1 would amplify many downstream effects. For example hyperacetylation of p53 result in increase in the gene expression of its various pro-apoptotic targets. In contrary SIRT1 deacetylate the p53, resulting in decrease in the expression of various pro-apoptotic targets. Thereby suppressing the apoptosis, similarly the activity of FOXO transcription factors was regulated *via* acetylation and deacetylation. It has been reported that SIRT1 inhibit the FOXO function thereby suppressing the apoptosis by blocking various pro-apoptotic genes like BIM, PUMA and TRAIL (FOXO transcription targets). In addition to that SIRT1 has its role in regulating the function of E2F1/p73 pathway, which was previously reviewed in detail [1,2]. This infers that SIRT1 inhibition could amplify the after effects significantly. We presume this could be the reason with the lower GIC_{50} values compared to the IC_{50} values of SIRT1 inhibitors.

3.6. Biological evaluation of SIRT1 activators

As discussed earlier SIRT1 activators were known to have important therapeutic intervention in obesity. Hence based on this presumption we had tested our compounds on adipocyte differentiation. Before performing the adipogenesis assay we tried to understand the cytotoxicity of these compounds (**A1**–**A5**) at 10 μM on adipocyte cell line utilizing MTT assay. From the result it was known that all the compounds except compound **A5** showed lesser cytotoxicity (Fig. 7). The percentage inhibition for the compounds **A1**–**A4** was less than 5%, hence they were believed to be non-toxic and further utilized for adipogenesis assay. Compound **A5** showed more than 40% inhibition. It was believed to cause lot of cell death and hence was inappropriate to be included for adipogenesis assay,

Table 4
Showing the GI_{50} of top five inhibitors on four different cell lines.

Compounds	GI_{50} values in μM				% Inhibition at 30 μM
	U937	MDAMB	LnCap	$CaCO_2$	HEK-293
I1	4.714 ± 2.36	0.7995 ± 0.19	0.2465 ± 0.078	0.01938 ± 0.0054	22.671 ± 2.37
I2	5.784 ± 2.34	16.69 ± 5.12	0.5309 ± 0.01	3.719 ± 1.12	20.697 ± 3.94
I3	51.53 ± 1.32	50.3 ± 1.43	0.07358 ± 0.001	0.06955 ± 0.009	25.874 ± 1.94
I4	18.42 ± 1.12	15.1 ± 2.76	0.003325 ± 0.001	0.5024 ± 0.0956	10.974 ± 2.89
I5	4.318 ± 0.12	1.246 ± 0.08	0.09673 ± 0.031	3.308 ± 1.23	30.474 ± 2.02 (CC_{50}: 40.12)
Gemcitabine	0.660 ± 0.02	0.050 ± 0.03	0.500 ± 0.02	0.042 ± 0.02	ND

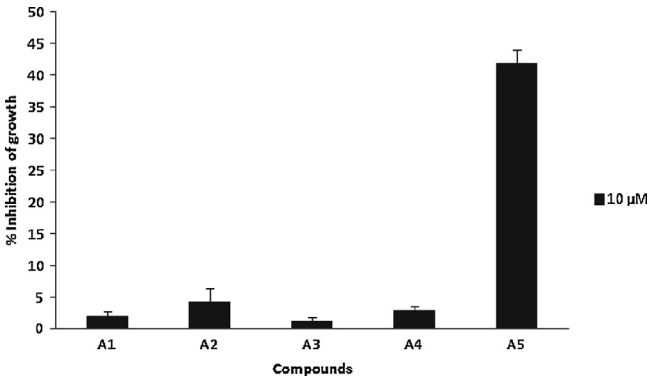

Fig. 7. Depicting the percentage of inhibition of SIRT1 activators on 3T3-L1 cell line at 10 μM concentration.

as it would interfere with the absorbance values. As this assay was based on colorimetric detection, reduction in the color may also be attributed to decrease in the cell number, which can be wrongly interpreted as decrease in the adipogenesis and hence compound **A5** was ignored for the adipogenesis assay. In order to understand the effects of SIRT1 activators on adipogenesis, the test compounds (**A1**–**A4**) were treated at two concentrations along with differentiation media. Relative lipid content was measured after staining with oil O red. Considering the lipid content in fully differentiating cells as 100%, relative percentage for drug treated cells was measured and presented in Fig. 8. From the assay results it was clear that approximately 40% reduction in lipid content was seen in all drug treated reactions. Prominently the reduction in lipid content was highly observed in **A2** treated wells. This inferred that **A2** was showing higher reduction in lipid content at both the concentrations (10 μM and 50 μM) relative to other test compounds. The activity was further supported with its docking score and *in vitro* enzyme activity which was relatively more to other test compounds. Hence it could be prominent to say that **A2** could be considered as best test compound among others.

As we know that obese individuals has increased number of adipocytes relative to the leaner individuals. Adipogenesis is an important mechanism which converts pre adipocytes into mature adipocytes. Mature adipocytes will have more fat droplets compared to the pre adipocytes. One of the critical elements in this process is PPAR-gamma, which induce adipogenesis. Without the function of PPAR-gamma pre adipoctyes could not get converted into mature adipoctyes. One of the important targets of SIRT1 is PPAR-gamma which deacetylates it and attenuates its functions. This infers that SIRT1 indirectly shows its effects on the adipogenesis. Since SIRT1 activators could reduce the adipogenesis, so as we observed in the results of adipogenesis assay. All the SIRT1 activators showed reduction in the lipid content (fat droplets) more than 40%, thus in the present study we could validate the link between SIRT1 activators and adipogenesis.

3.7. Drug likeliness of the designed inhibitors and activators

The drug likeness properties of the top leads were predicted by using QikProp module (Table 5) from Schrodinger. All top leads showed good partition coefficient (QPlogP0/w) and values were within the acceptable range of −2.0 to 6.5. In addition QPlogS was determined to know the aqueous solubility. All the leads were in the range of −6.4 to −3.4. **I3** and **A2** showed values above the acceptable range (−6.5 to 0.5) and hence might show issues with solubility. Predicted Caco-2 cell permeability was in the range of 0.1 to 747 nm/s, with **I3** and **A2**, with a low cell permeability of <25 nm/s. The percentage of human oral absorption for compounds ranged from 1% to 100%, with compound **A2** with least

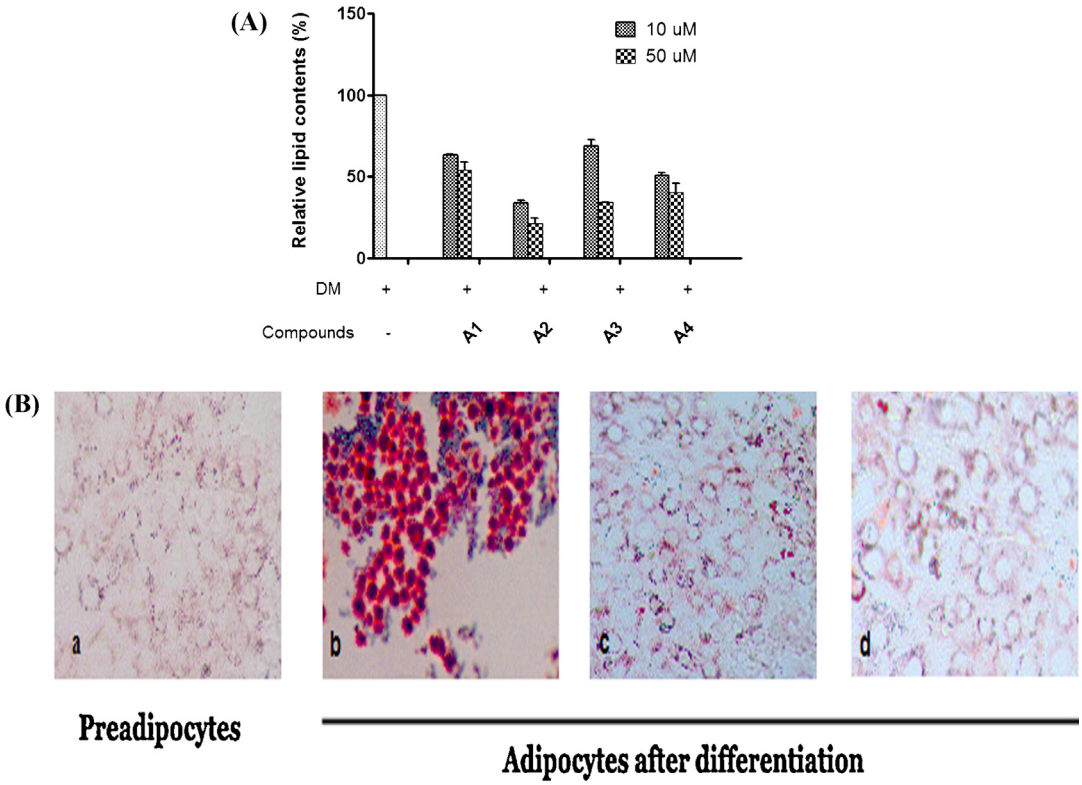

Fig. 8. (A) Depicting the relative lipid content of cells after treatment with test compounds with respective of cells untreated and (B) illustrating the lipid content of the cell after staining with oil O red, were a, b, c and d represents preadipocytes, differentiated adipocytes, cell treated with A2 at 10 μM and cells treated with A2 at 50 μM, respectively.

Table 5
Represents the predictive pharmacokinetic properties of top leads.

Title	QPlogP0/w[a]	QPlogS[b]	QPPCaco[c]	% Human oral absorption[d]	Rule of five[e]
I1	0.224	−4.9	32.535	35.486	0
I2	2.388	−4.163	159.254	80.343	0
I3	3.837	−6.334	0.341	38.099	1
I4	3.243	−3.214	201.873	78	0
I5	3.804	−4.313	747.992	100	0
A1	2.702	−4.739	121.1	80.049	0
A2	2.757	−6.423	21.127	21.147	2
A3	3.903	−5.698	305.644	94.282	0
A4	2.101	−3.523	342.597	84.618	0
A5	0.25	−4.478	39.292	51.416	0

[a] Predicted octanol/water partition co-efficient log *p* (acceptable range from −2.0 to 6.5).
[b] Predicted aqueous solubility, log *S* (acceptable range from −6.5 to 0.5).
[c] Predicted Caco-2 cell permeability in nm/s (acceptable range: <25 is poor and >500 is great).
[d] Percentage of human oral absorption (<25% is poor and >80% is high).
[e] Number of violations of Lipinski's rule of five (maximum is 4).

oral absorption (21%) which could be attributed to its bulky size. There were only two compounds (**I3** and **A2**) which showed 1 or 2 violations of Lipinski rule of five. Therefore among all the lead molecules **I3** and **A2** were found to have molecular weight more than 500 Da. Never the less these properties could be modified by altering the functional groups in order to make the compounds less bulky and with better pharmacokinetic properties.

4. Conclusion

SIRT1 being the most important regulator of metabolism, both activators and inhibitors are important in treating various metabolic disorders. The present work focuses on discovering novel modulators, which would help in further development of future drugs. In conclusion we have found a new compound **A2** (activator) using homology model published earlier [17], which showed good activity both in enzyme and cell based studies. These results further inferred that the homology model developed by Autiero et al., can be used to screen small molecule SIRT1 activators. Besides we had also discovered a new inhibitor **I1** with IC_{50} value of 16.35 μM and moderate activity in cancer cell lines. Further to this in the process of discovery we also discovered a new compound **I5** with moderate activity on SIRT1 enzyme but potentially promising effect on prostate cancer cell line with GI_{50} value of 96 nM, which was supported by cell cycle analysis studies. Further work is in progress to increase the possibility of affinity of these lead modulators through structural modification and developing structure–activity relationship. Novel strategies like e-pharmacophore and ligand based drug design could be employed to design novel inhibitors against SIRT1. Potential other targets of **I5** can be explored by screening this compound on various sirtuins.

Acknowledgement

This study was supported by grants from Department of Biotechnology (DBT) with the sanction order number: BT/PR13326/BRB/10/49/2009, Government of India.

References

[1] M.C. Haigis, L.P. Guarente, Mammalian sirtuins: emerging roles in physiology, aging, and calorie restriction, Genes Dev. 20 (21) (2006) 2913–2921.
[2] B.J. North, B.L. Marshall, M.T. Borra, J.M. Denu, E. Verdin, The human Sir2 ortholog, SIRT2 is an NAD+-dependent tubulin deacetylase, Mol. Cell 11 (2) (2003) 437–444.
[3] G. Donmez, L. Guarente, Aging and disease: connections to sirtuins, Aging Cell 9 (2) (2010) 285–290.
[4] K.M. Ramsey, K.F. Mills, A. Satoh, S.I. Imai, Ageing Cell 7 (2008) 78–88.
[5] M.C. Haigis, D.A. Sinclair, Mammalian sirtuins: biological insights and disease relevance, Annu. Rev. Pathol. 5 (2010) 253;
R.C. Neugebauer, W. Sippl, M. Jung, Inhibitors of NAD+ dependent histone deacetylases (sirtuins), Curr. Pharm. Des. 14 (2008) 562–573.
[6] R.C. Neugebauer, U. Uchiechowska, R. Meier, H. Hruby, V. Valkov, E. Verdin, W. Sippl, M. Jung, Structure–activity studies on splitomicin derivatives as sirtuin inhibitors and computational prediction of binding mode, J. Med. Chem. 51 (5) (2008) 1203–1213.
[7] A.D. Napper, J. Hixon, T. McDonagh, K. Keavey, J.-F. Pons, J. Barker, W.T. Yau, P. Amouzegh, A. Flegg, E. Hamelin, Discovery of indoles as potent and selective inhibitors of the deacetylase SIRT1, J. Med. Chem. 48 (25) (2005) 8045–8054.
[8] A. Bedalov, T. Gatbonton, W.P. Irvine, D.E. Gottschling, J.A. Simon, Identification of a small molecule inhibitor of Sir2p, Proc. Natl. Acad. Sci. U. S. A. 98 (26) (2001) 15113–15118.
[9] J. Posakony, M. Hirao, S. Stevens, J.A. Simon, A. Bedalov, Inhibitors of Sir2: evaluation of splitomicin analogues, J. Med. Chem. 47 (10) (2004) 2635–2644.
[10] A. Mai, S. Massa, S. Lavu, R. Pezzi, S. Simeoni, R. Ragno, F.R. Mariotti, F. Chiani, G. Camilloni, D.A. Sinclair, Design, synthesis, and biological evaluation of sirtinol analogues as class III histone/protein deacetylase (Sirtuin) inhibitors, J. Med. Chem. 48 (24) (2005) 7789–7795.
[11] F. Medda, R.J. Russell, M. Higgins, A.R. McCarthy, J. Campbell, A.M. Slawin, D.P. Lane, S. Lain, N.J. Westwood, Novel cambinol analogs as sirtuin inhibitors: synthesis, biological evaluation, and rationalization of activity, J. Med. Chem. 52 (9) (2009) 2673–2682.
[12] T. Suzuki, K. Imai, H. Nakagawa, N. Miyata, 2-Anilinobenzamides as SIRT inhibitors, ChemMedChem 1 (10) (2006) 1059–1062.
[13] C. Gey, S. Kyrylenko, L. Hennig, L.H.D. Nguyen, A. Büttner, H.D. Pham, A. Giannis, Phloroglucinol derivatives guttiferone G, aristoforin, and hyperforin: inhibitors of human sirtuins SIRT1 and SIRT2, Angew. Chem. Int. Ed. 46 (27) (2007) 5219–5222.
[14] P.H. Kiviranta, J. Leppänen, V.M. Rinne, T. Suuronen, O. Kyrylenko, S. Kyrylenko, E. Kuusisto, A.J. Tervo, T. Järvinen, A. Salminen, N-(3-(4-hydroxyphenyl)-propenoyl)-amino acid tryptamides as SIRT2 inhibitors, Bioorg. Med. Chem. Lett. 17 (9) (2007) 2448–2451.
[15] B.D. Sanders, B. Jackson, R. Marmorstein, Structural basis for sirtuin function: what we know and what we don't, Biochim. Biophys. Acta 1804 (8) (2010) 1604–1616.
[16] T. Huhtiniemi, C. Wittekindt, T. Laitinen, J. Leppänen, A. Salminen, A. Poso, M. Lahtela-Kakkonen, Comparative and pharmacophore model for deacetylase SIRT1, J. Comput. Aided Mol. Des. 20 (9) (2006) 589–599.
[17] I. Autiero, S. Costantini, G. Colonna, Human sirt-1: molecular modeling and structure-function relationships of an unordered protein, PLoS ONE 4 (10) (2009) e7350.
[18] X. Zhao, D. Allison, B. Condon, F. Zhang, T. Gheyi, A. Zhang, S. Ashok, M. Russell, I. MacEwan, Y. Qian, The 2.5 Å crystal structure of the SIRT1 catalytic domain bound to nicotinamide adenine dinucleotide (NAD+) and an indole (EX527 analogue) reveals a novel mechanism of histone deacetylase inhibition, J. Med. Chem. 56 (3) (2013) 963–969.
[19] M.S. Finnin, J.R. Donigian, N.P. Pavletich, Structure of the histone deacetylase SIRT2, Nat. Struct. Biol. 8 (7) (2001) 621–625, http://dx.doi.org/10.1038/89668.
[20] M.T. Borra, B.C. Smith, J.M. Denu, Mechanism of human SIRT1 activation by resveratrol, J. Biol. Chem. 280 (17) (2005) 17187–17195.
[21] J.L. Avalos, J.D. Boeke, C. Wolberger, Structural basis for the mechanism and regulation of Sir2 enzymes, Mol. Cell 13 (5) (2004) 639–648.
[22] K. Zhao, X. Chai, R. Marmorstein, Structure of the yeast Hst2 protein deacetylase in ternary complex with 2′-O-acetyl ADP ribose and histone peptide, Structure 11 (11) (2003) 1403–1411.
[23] A. Sharma, V. Gautam, S. Costantini, A. Paladino, G. Colonna, Interactomic and pharmacological insights on human Sirt-1, Front. Pharmacol. 3 (2012) 40–43.
[24] J.C. Milne, P.D. Lambert, S. Schenk, D.P. Carney, J.J. Smith, D.J. Gagne, L. Jin, O. Boss, R.B. Perni, C.B. Vu, Small molecule activators of SIRT1 as therapeutics for the treatment of type 2 diabetes, Nature 450 (7170) (2007) 712–716.
[25] M. Pacholec, J.E. Bleasdale, B. Chrunyk, D. Cunningham, D. Flynn, R.S. Garofalo, D. Griffith, M. Griffor, P. Loulakis, B. Pabst, SRT1720, SRT2183, SRT1460, and resveratrol are not direct activators of SIRT1, J. Biol. Chem. 285 (11) (2010) 8340–8351.

[26] M. Lakshminarasimhan, D. Rauh, M. Schutkowski, C. Steegborn, Sirt1 activation by resveratrol is substrate sequence-selective, Aging (Albany, NY) 5 (3) (2013) 151.
[27] B.P. Hubbard, A.P. Gomes, H. Dai, J. Li, A.W. Case, T. Considine, T.V. Riera, J.E. Lee, S. Yen, D.W. Lamming, Evidence for a common mechanism of SIRT1 regulation by allosteric activators, Science 339 (6124) (2013) 1216–1219.
[28] H. Dai, L. Kustigian, D. Carney, A. Case, T. Considine, B.P. Hubbard, R.B. Perni, T.V. Riera, B. Szczepankiewicz, G.P. Vlasuk, SIRT1 activation by small molecules kinetic and biophysical evidence for direct interaction of enzyme and activator, J. Biol. Chem. 285 (43) (2010) 32695–32703.
[29] V.K. Pulla, M.B. Battu, M. Alvala, D. Sriram, P. Yogeeswari, Can targeting SIRT-1 to treat type 2 diabetes be a good strategy? A review, Expert Opin. Ther. Targets 16 (8) (2012) 819–832.
[30] LigPrep, Version 2.5, Schrodinger, LLC, New York, NY, 2011.
[31] Canvas, Version 1.4, Schrodinger, LLC, New York, NY, 2011.
[32] R.A. Friesner, J.L. Banks, R.B. Murphy, T.A. Halgren, J.J. Klicic, D.T. Mainz, M.P. Repasky, E.H. Knoll, M. Shelley, J.K. Perry, Glide – a new approach for rapid, accurate docking and scoring: 1. Method and assessment of docking accuracy, J. Med. Chem. 47 (7) (2004) 1739–1749.
[33] V.M. Nayagam, X. Wang, Y.C. Tan, A. Poulsen, K.C. Goh, T. Ng, H. Wang, H.Y. Song, B. Ni, M. Entzeroth, SIRT1 modulating compounds from high-throughput screening as anti-inflammatory and insulin-sensitizing agents, J. Biomol. Screen. 11 (8) (2006) 959–967.
[34] J.A. Plumb, Cell sensitivity assays: the MTT assay, in: Cancer Cell Culture, Springer, Totowa, NJ, 2004, pp. 165–169.
[35] M.-S. Kim, J.-K. Kim, D.-Y. Kwon, R. Park, Anti-adipogenic effects of *Garcinia* extract on the lipid droplet accumulation and the expression of transcription factor, Biofactors 22 (1) (2004) 193–196.
[36] Y. Zhang, Y. Cheng, X. Ren, T. Hori, K.J. Huber-Keener, L. Zhang, K.L. Yap, D. Liu, L. Shantz, Z.-H. Qin, Dysfunction of nucleus accumbens-1 activates cellular senescence and inhibits tumor cell proliferation and oncogenesis, Cancer Res. 72 (16) (2012) 4262–4275.
[37] J.-H. Chang, H.-C. Kim, K.-Y. Hwang, J.-W. Lee, S.P. Jackson, S.D. Bell, Y. Cho, Structural basis for the NAD-dependent deacetylase mechanism of Sir2, J. Biol. Chem. 277 (37) (2002) 34489–34498.